ChemComm

Accepted Manuscript

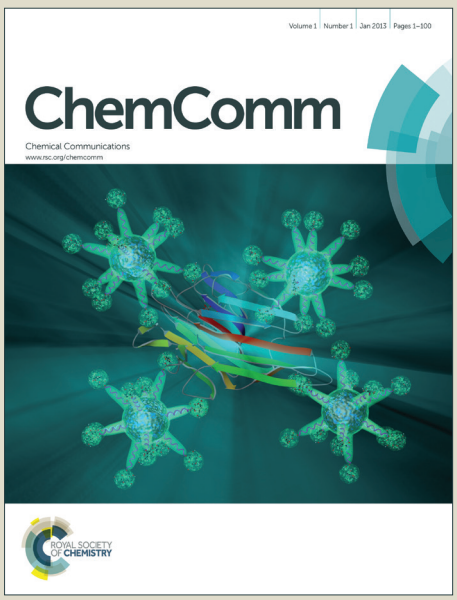

ROYAL SOCIETY OF CHEMISTRY

www.rsc.org/chemcomm

Journal Name

RSCPublishing

COMMUNICATION

The first 4d/4f single-molecule magnet containing a $\{Ru^{III}_2Dy^{III}_2\}$ core†

Add tCite this: DOI: 10.1039/x0xx00000x

Stuart K. Langley,[a] Daniel P. Wielechowski,[a] Veacheslav Vieru,[b] Nicholas F. Chilton,[c] Boujemaa Moubaraki,[a] Liviu F. Chibotaru[b*] and Keith S. Murray[a*]

Received 00th January 2012,
Accepted 00th January 2012

DOI: 10.1039/x0xx00000x

www.rsc.org/

We report the synthesis, structure and magnetic properties of the first 4d-4f single-molecule magnet. The complex $[Ru^{III}_2Dy^{III}_2(OMe)_2(O_2CPh)_4(mdea)_2(NO_3)_2]$ displays a butterfly type core, with an anisotropy barrier of 10.7 cm^{-1}. *Ab initio* and DFT calculations provide insight into the observed magnetic behaviour.

Single-molecule magnets (SMMs) are a class of zero-dimensional compounds with a wide range of properties such as magnetic bistability below a blocking temperature, the ability to exhibit quantum tunnelling of the magnetization (QTM) and quantum coherence.[1] SMMs have gained great interest due to potential technological applications such as storing and processing digital information,[2] and as molecular spintronic devices.[3] Anisotropic 4f ions[4] have been used to improve upon the properties laid out by the first generation SMMs, which were based on polynuclear 3d complexes, namely the hysteretic blocking temperature (T_B) and anisotropy barrier (U_{eff}).[5] A drawback in the use of lanthanide ions is that the magnetic super-exchange interaction(s) between Ln^{III} ions in polynuclear complexes are very small. As a consequence we are restricted to the electronic structure of essentially a single ion. Moreover fast QTM is often observed, an undesired property for magnetic bistability as it decreases relaxation times.[6] In order to overcome these drawbacks, a few groups have shifted towards the use of 4d and 5d ions as these ions are highly anisotropic, with more diffuse d orbitals that may promote stronger magnetic exchange than the corresponding 3d-4f and 4f-4f counterparts. Indeed it was recently found that the anti-symmetric exchange introduced by Ru^{III} ions was responsible for large magnetic anisotropy in a $\{Ru_2Mn\}$ triangle and extremely strong exchange was realized ($J > -1000$ cm^{-1}) in a $\{Ru^{III}_6\}$ complex.[7] Dunbar et al have reviewed heterometallic 3d-4d, 3d-5d and homometallic 4d and 5d compounds, utilizing ions such as Ru^{III}, Mo^{III}, Mo^{V}, Re^{IV}, Os^{III} and W^{V}, with a number of these displaying SMM behaviour.[8] This review notwithstanding, the magneto-chemistry of Ln^{III} complexes containing 4d and 5d ions remain little studied, and may be due to the complicated nature of the magnetic anisotropy and the difficulty in modelling the magnetic data. Recent advances in *ab initio* calculations have proven invaluable in the advancement of our understanding of slow magnetic relaxation in anisotropic 4f coordination compounds.[9] With this background in mind, we aimed to synthesize new 4d and/or 5d containing clusters with a view to making a theoretical analysis of the magnetic properties and establish some guiding principles and elucidate what factors may allow for the observation of SMM behaviour using 4d or 5d ions. We chose the 4d ion Ru^{III} as starting point for this work. Several 3d-Ru^{III} complexes have recently been isolated,[8] with a $\{Mn^{III}_2Ru^{III}\}$ complex displaying slow relaxation of the magnetization.[10] Here we incorporate the 4d Ru^{III} ion into a Dy^{III} complex and report the synthesis, structure, magnetic characterization and an *ab initio* and DFT theoretical analysis of a new Ru^{III} based SMM.

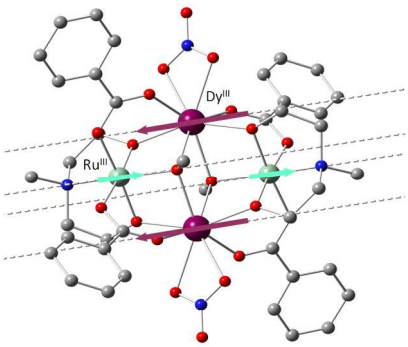

Fig. 1. Molecular structure of **1**. The H atoms are omitted for clarity. Colour scheme; Ru^{III}, pale green; Dy^{III}, purple; O, red; N, blue; C, light grey. The dashed lines correspond to the main magnetic axes of the Dy^{III} ions and the axes perpendicular to the anisotropy plane of the Ru^{III} ions. The arrows show the orientation of local magnetic moments in the ground exchange doublet state.

The reaction of $RuCl_3{\cdot}6H_2O$, $Dy(NO_3)_3{\cdot}6H_2O$, benzoic acid, N-methyldiethanolamine ($mdeaH_2$) and triethylamine in acetonitrile resulted in a brown solution. Yellow crystals of $[Ru^{III}_2Dy^{III}_2(OMe)_2(O_2CPh)_4(mdea)_2(NO_3)_2]$ (**1**) were subsequently

isolated (see ESI for experimental details). Complex **1** (Fig. 1) crystallizes in the monoclinic space group $P2_1/n$, with the asymmetric unit containing half the cluster (one Ru^{III} and Dy^{III} ion), which lies upon an inversion centre (see ESI and Table S1 for X-ray details). Overall, **1** is a tetranuclear complex consisting of two Ru^{III} and two Dy^{III} ions, with the metallic core displaying a butterfly type arrangement. The Dy^{III} ions occupy the body (central) sites, with the Ru^{III} ions occupying the outer wing positions. The Ru^{III} and Dy^{III} ions are bridged via two μ_3 methoxide ligands, each coordinating the two Dy^{III} ions to a single Ru^{III} ion. The complex is further stabilized by two $[mdea]^{2-}$ ligands, each of which coordinate via the N-atom to a Ru^{III} ion and then bridge via the two μ_2-O atoms to a Ru^{III} and a Dy^{III} ion. Four benzoate ligands each bridge a Ru^{III} to a Dy^{III} ion with the common μ *syn-syn* bridging mode. The coordination sphere for each Dy^{III} ion is completed by a single chelating nitrate ligand. The Ru^{III} ions are six-coordinate with distorted octahedral geometries, and an average Ru-$L_{N,O}$ bond distance of 2.04 Å. The Dy^{III} ions are both eight-coordinate, and display distorted square-antiprismatic geometries, quantified by SHAPE analysis, with a CShM of 1.637. The average Dy-O bond length is 2.36 Å. Selected bond lengths and angles are given in Table S2. Packing diagrams are shown in Fig. S1. Compound **1** is isostructural to $\{Co^{III}_2Dy^{III}_2\}$ and $\{Cr^{III}_2Dy^{III}_2\}$ SMMs.[11,12]

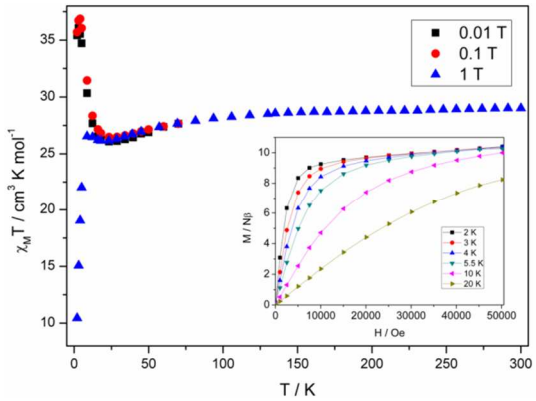

Fig. 2. Plot of $\chi_M T$ *versus* T for **1** measured under a 1 (300 to 2 K), 0.1 and 0.01 T (70 to 2 K) magnetic fields; (Inset) Isothermal M *versus* H plots for **1** at the temperatures shown.

Direct current (dc) susceptibility measurements on a polycrystalline sample of **1** in the temperature range 2 – 300 K yield the $\chi_M T$ (χ_M = molar magnetic susceptibility) *versus* T plot (Fig. 2), with a $\chi_M T$ value of 29.01 cm^3 K mol^{-1} at 300 K. This is close to the expected value of 29.09 cm^3 K mol^{-1} for an uncoupled $\{Ru^{III}_2Dy^{III}_2\}$ moiety. As the temperature is decreased the $\chi_M T$ product decreases gradually down to 25 K, below which an upturn is observed. The low temperature behaviour is field dependent, with a further decrease observed under all fields at the lowest temperatures measured due to Zeeman depopulation effects. The high temperature decrease (300 – 25 K) is due to the depopulation of the excited m_J states of the Dy^{III} ions, while the increase at lower temperatures suggests non-negligible exchange interactions between the Ru^{III} and the Dy^{III} ions (see *ab initio* and DFT analysis). The isothermal magnetization (M) measurements (Fig. 2, inset) each display a rapid increase in magnetization below 2 T, before a more gradual linear-like increase, without saturating. This suggests a significant magnetic anisotropy is present. We therefore examined for M vs H hysteresis, however, no coercivity was observed down to 1.8 K (4 Oe/s) (Fig. S2) using a conventional SQUID magnetometer.

In order to probe for slow magnetic relaxation on a shorter timescale, above 1.8 K, variable temperature and variable frequency alternating current (ac) susceptibility measurements were performed with an oscillating ac field of 3.5 Oe under a zero applied dc field. These measurements revealed frequency and temperature dependence of both

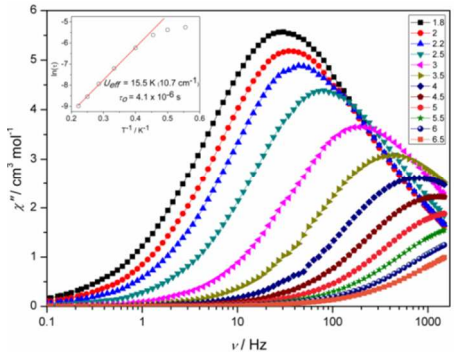

Fig. 3. Frequency dependence of χ_M'' for **1**, with H_{ac} = 3.5 Oe and H_{dc} = 0 Oe; (inset) Relaxation data plotted as ln(τ) versus T^{-1}.

the in-phase (χ_M') (Fig. S3) and out-of-phase (χ_M'') (Fig. 3 and Fig. S4) susceptibility components, signifying SMM behaviour. Cole-Cole plots of χ_M' *versus* χ_M'', (Fig. S5) reveal semi-circular profiles thus indicating a single relaxation process is operative. The plots were fitted to a generalized Debye model with α parameters in the range 0.14 – 0.34 between 9 and 1.8 K, indicating a moderate distribution of relaxation times at the lowest of temperatures. The relaxation times (τ) are temperature dependent between 1.8 – 4.5 K, and reveal a linear dependence between 2.5 – 4.5 K, when plotted as ln(τ) *versus* $1/T$ (Fig. 3, inset). Fitting the data to the Arrhenius law [$\tau = \tau_o exp(U_{eff}/k_BT)$] yields an anisotropy barrier U_{eff} = 16(1) K (~ 11 cm^{-1}), with τ_0 = 4.1 x 10^{-6} s (see ESI for comment on the τ_0 value). Below 2.5 K the relaxation time deviates from linearity, crossing over from a thermally activated to a quantum regime, with τ_{QTM} ~ 5 ms. Compound **1** is the first reported 4d/4f SMM.

Comparing the $\{Ru^{III}_2Dy^{III}_2\}$ experimental magnetic data to the isostructural 3d based $\{Co^{III}_2Dy^{III}_2\}$ and $\{Cr^{III}_2Dy^{III}_2\}$ butterfly complexes, we observe marked differences in the magnetic relaxation data.[11,12] The Co^{III} family displayed anisotropy barriers (U_{eff}) in the thermally activated regime (> 8 K) of 55 – 80 cm^{-1}, while in the low temperature domain, relaxation via QTM was dominant, with fast tunnelling times in the range of 0.1 – 1.5 s. In these complexes it was found that the relaxation originates from a single Dy^{III} ion because of minimal Dy^{III} – Dy^{III} exchange interactions (<|0.6| cm^{-1}).[11a] Replacement of the diamagnetic Co^{III} with the paramagnetic Cr^{III} ion gave a similar relaxation barrier for the $mdeaH_2$ analogue (~ 55 cm^{-1}) cf. Co^{III}, however, a significant increase in relaxation times was observed at temperatures below 6 K. This allowed for the observation of highly coercive magnetic hysteresis loops, open up to 3.7 K, a feature not present in the Co^{III} case(s). The increase in relaxation times despite similar barrier heights was attributed to the strong magnetic exchange between the Cr^{III} and Dy^{III} ions (~|17-20| cm^{-1}), relative to the weak Dy-Dy exchange (<|0.6| cm^{-1}).[12] From this result, and moving down a period, with the greater radial extension of the 4d orbitals, we may

expect even stronger magnetic exchange,[7] and thus the potential for longer relaxation times.[13] However the experimental data reveals that the relaxation barrier is much smaller, at 10.7 cm^{-1}, and as a consequence fast(er) relaxation times are observed at the temperatures studied, hence no *M* vs *H* coercivity was found above 1.8 K. The α parameters for the $\{Cr_2Dy_2\}$ analogue are 0.12 and 0.28 at 8.5 and 5.0 K, being larger at 5 K than for $\{Ru_2Dy_2\}$, the latter showing increases in α at 1.8 K due to QTM.

To quantify these observations, *ab initio* and DFT calculations were performed using MOLCAS 7.8[14] and ORCA 2.9.0[15] software, respectively. Details are given in the ESI and Table S3. Fragment CASSCF/SO-RASSI/SINGLE_ANISO[16] type calculations have been performed to determine the low-lying energy levels and magnetic properties of individual Dy^{III} and Ru^{III} centres. Only one Dy^{III} and Ru^{III} centre per complex has been calculated, due to the presence of the inversion centre. Table S4 shows that the ground state for the Ru^{III} ion is a doublet, which is expected due to the strong crystal field splitting of the 4d orbitals. This is backed up via DFT (BP and B3LYP) calculations (Table S5). Table 1 shows the energies of the lowest Kramers doublets of the individual Dy^{III} and Ru^{III} ions and the *g* tensors of the ground Kramers doublet. The significant anisotropy of the Ru^{III} S = $^1/_2$ ground state is due to the strong spin-orbit coupling despite the quenched orbital angular momentum in the ground state.

Table 1. Energies of the lowest Kramers doublets (cm^{-1}) of Dy^{III} and Ru^{III} centres and the *g* tensor of the ground Kramers doublet.

Spin-orbit energies, cm^{-1}			
Dy		Ru	
Dy_basis1	Dy_basis2	Ru_basis1	Ru_basis2
0	0	0	0
179	146	3972	4197
278	216	5115	5264
306	250	15188	15571
319	264	15260	15634
379	329	15411	15802
423	367	15607	15965
546	555	17874	18376
g_x = 0.0051	g_x = 0.0079	g_x = 2.65	g_x = 2.60
g_y = 0.0057	g_y = 0.0095	g_y = 2.48	g_y = 2.47
g_z = 19.74	g_z = 19.76	g_z = 1.54	g_z = 1.58

The ground KD for the Dy^{III} sites are highly axial, while the ground KD of Ru^{III} displays easy anisotropy plane of magnetization, which is much weaker than the anisotropy on the Dy^{III} sites (Table 1). Consequently, it is the latter which defines the SMM behaviour of the complex.

In order to gain some information about the exchange coupling constants in this system we performed BS-DFT calculations at the B3LYP/SVP level. To estimate the exchange constant for all pairs, we performed calculations on model complexes with the experimental geometry. To examine the exchange between the Ru^{III} ions we substituted Dy^{III} ions for Lu^{III}, giving a $\{Lu^{III}_2Ru^{III}_2\}$ complex. To investigate the exchange interaction between the Dy^{III} ions we substituted Ru^{III} for Y^{III} and Dy^{III} for Gd^{III}, giving a $\{Gd^{III}_2Y^{III}_2\}$ complex; the exchange parameters were then rescaled for the spin *S* = $^5/_2$ of dysprosium ions compared to the *S* = $^7/_2$ of gadolinium. Finally, to examine the Dy^{III} – Ru^{III} interactions, we performed calculations on two complexes of the type {Gd(1)Lu(1')Ru(1)Y(1')} and {Gd(1)Lu(1')Y(1)Ru(1')}, with subsequent rescaling to the spin of Dy^{III}. In all cases we applied Yamaguchi's formula to estimate the exchange coupling constants.[17] The following Hamiltonian was employed to account for exchange interactions, where the interactions with the orbitally degenerate Dy^{III} ions was accounted for within the Lines model[18]:

$$\hat{H}_{exch} = -J_{Ru-Ru}\hat{S}_{Ru}\cdot\hat{S}_{Ru} - J_{Dy-Dy}\hat{S}_{Dy}\cdot\hat{S}_{Dy} - 2J_{Dy1-Ru1}\hat{S}_{Dy}\cdot\hat{S}_{Ru} - 2J_{Dy1-Ru1'}\hat{S}_{Dy}\cdot\hat{S}_{Ru} \quad \text{(Eq.1)}$$

where $\hat{S}$ are the spin operators of the Dy^{III} and Ru^{III} ions, respectively, $S_{Dy} = 5/2$, $S_{Ru} = 1/2$. The obtained exchange parameters are shown in Table 2.

Magnetic susceptibility data, $\chi_M T(T)$, (Fig. S7) and the $M(H)$ curves (Fig. S8) were calculated using the DFT determined exchange parameters and including the dipolar interaction. The employed Hamiltonian including exchange and dipolar interactions is of the same

Table 2. Exchange parameters (cm^{-1}) between magnetic ions for the $\{Ru^{III}_2Dy^{III}_2\}$ complex **1**.

Pair	Calculated	Fitted
	J_{Lines}	J_{Lines}
Dy1-Dy1'	0	0
Ru1-Ru1'	-0.4	-0.4
Dy1-Ru1	-3.7	-3.7
Dy1-Ru1'	-3.5	-3.5

form as the one used for description of $\{Cr^{III}_2Dy^{III}_2\}$ complex.[12] The DFT determined values give a good agreement of the calculated $\chi_M T$ curve with the experimental one, the only fitting parameter being used the intermolecular interaction *zJ'*, which is -0.021 cm^{-1}. The dominant exchange parameters are found between the Dy^{III} and Ru^{III} ions and are antiferromagnetic in nature. Due to the strong exchange interaction between Dy^{III} and Ru^{III} ions, the local magnetic moments in the ground exchange doublet state of Ru^{III} centres are aligned along the main anisotropy axes of Dy^{III} sites (Fig. 1). If we rescale the exchange coupling constants for Dy-Ru pairs (Table 2) to the pseudospin ½ of Dy ions and to the spin 3/2 of Cr ions from the $\{Cr^{III}_2Dy^{III}_2\}$ butterfly complex,[12] we obtain the following parameters: -5.8 and -6.2 cm^{-1}, which are smaller than the same parameters in $\{Cr^{III}_2Dy^{III}_2\}$ complex, -17 and -20 cm^{-1}, respectively. Following a recently proposed methodology, the obtained spectrum of exchange multiplets together with matrix elements of magnetic moments on the corresponding wave functions can be used for the construction of the barrier of reversal of magnetization.[12,19]

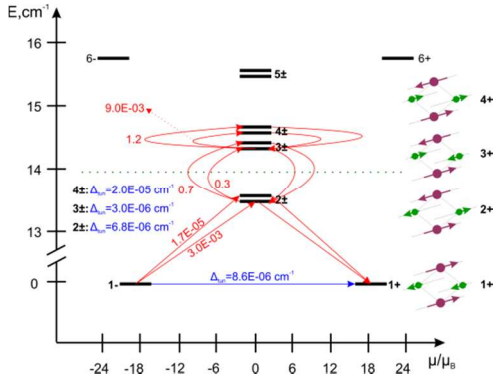

Fig. 4. *Ab initio* constructed barrier of relaxation of magnetization. On the right side the local magnetic moments shown for one of two components for each exchange doublet state.

The low-lying exchange spectrum and the position of the magnetization blocking barrier (dotted line) are shown in Fig. 4. The exchange states are placed on the diagram according to their magnetic moments (bold black lines). The horizontal blue arrows show the tunnelling transitions (the energy splitting) within each doublet state, while the non-horizontal arrows show the spin-phonon transition paths. The numbers at the paths are averaged transition moments in μ_B connecting the corresponding states. Red arrows correspond to the maximal transition probability from a given state, thus outlining the relaxation barrier within the ground exchange doublet. The barrier is of the exchange type, since multiple relaxation paths are involved between several exchange levels (Fig. 4). We would like to stress that the magnetic blocking barrier is constructed without using any fitting parameter other than *zJ'* to account for intermolecular interaction. The *ab initio* built blocking barrier is in excellent agreement (13.9 cm^{-1}) with the experimentally determined value (~11 cm^{-1}). However, the barrier in **1** is significantly smaller than in the isostructural $\{Cr^{III}_2Dy^{III}_2\}$ complex.[12] This can be explained by two reasons. First, the exchange interaction between the Dy-Ru pairs is weaker than for the Dy-Cr pairs. Since in both complexes the barrier is of the exchange type, it is clear that a weaker exchange interaction would lower the barrier in one of them. Secondly, the spin of Cr is 3/2, whereas the spin of Ru is ½. Therefore, the chromium complex possesses more exchange doublet states and involves, therefore, more levels in the blocking barrier (c.f. the present Fig. 4 and the Fig. 6 in Ref. [12]). A similar situation was observed in a series of $\{Co^{II}\text{-}Ln^{III}\text{-}Co^{II}\}$, Ln = Gd, Tb and Dy, where the Gd complex was found to be a much better SMM.[19] Comparing $\{Cr^{III}_2Dy^{III}_2\}$[12] with **1** shows that the best SMM effect is achieved via an efficient interaction between anisotropic metal ions with a strongly axial ground state and *high-spin* isotropic metal ions.[19]

In summary, we have synthesised a rare Ru^{III}-based polynuclear complex that is the first 4d/4f SMM. Calculations reveal significant Ru-Dy magnetic exchange interactions of -3.5 and -3.7 cm^{-1}, stronger than usually observed for 4f-4f and the majority of reported 3d-4f complexes.[11] It is this reason that a thermally activated slow relaxation mechanism is observed in the absence of a static dc field, and stems from an exchange based multilevel mechanism, with only a cross over to a quantum regime observed below 2.5 K (c.f. $\{Co^{III}_2Dy^{III}_2\}$ complexes, with negligible exchange, where QTM is observed from ~8 K). For **1**, however, the Ru-Dy pair-wise exchange parameter is smaller than the Cr-Dy pair-wise exchange in an isostructural analogue and this is the major reason for the smaller anisotropy barrier (11 vs 55 cm^{-1}). This work highlights that 4d ions can be used to develop new SMMs and will be integral for the targeted synthesis of future heterometallic lanthanide complexes that exhibit strong magnetic exchange interactions and long relaxation times.

Notes and references

[a] School of Chemistry, Monash University, Clayton, Victoria 3800, Australia. email: keith.murray@monash.edu

[b] Theory of Nanomaterials Group and INPAC - Institute of Nanoscale Physics and Chemistry, Katholieke Universiteit Leuven, Celestijnenlaan 200F, 3001 Heverlee, Belgium. email: Liviu.Chibotaru@chem.kuleuven.be

[c] School of Chemistry, The University of Manchester, Manchester M13 9PL, U.K.

† CCDC number 1032631. Electronic Supplementary Information (ESI) available: [experimental details, magnetic data and computational details and information]. See DOI: 10.1039/c000000x/.

1. G. Christou, D. Gatteschi and D. N. Hendrikson, R. Sessoli, *MRS Bull.*, 2000, 725.
2. (a) M. N. Leuenberger, D. Loss, Nature, 2001, **410**, 789; (b) A. Ardavan, O. Rival,J. J. L. Morton, S. J. Blundell, A. M. Tyryshkin, G. A. Timco and R. E. P. Winpenny, *Phys. Rev. Lett.*, 2007, **98**, 057201.
3. M. Urdampilleta, N. V. Nguyen, J. P. Cleuziou, S. Klyatskaya, M. Ruben and W. Wernsdorfer, *Int. J. Mol. Sci*., 2011, **12**, 6656
4. D. N. Woodruff, R. E. P. Winpenny and R. A. Layfield, *Chem. Rev*., 2013, **113**, 5110.
5. G. Aromi and E. K. Brechin, *Struct. Bonding*, 2006, **122**, 1.
6. S. K. Langley, N. F. Chilton, B. Moubaraki and K. S. Murray, *Inorg. Chem*., 2013, **52**, 7183.
7. (a) A. Upadhyay, J. Rajpurohit, M. K. Singh, R. Dubey, A. K. Srivastava, A. Kumar, G. Rajaraman, and M. Shanmugam, *Chem. Eur. J*., 2014, **20**, 6061; (b) S. A. Magee, S. Sproules, A.-L. Barra, G. A. Timco, N. F. Chilton, D. Collison, R. E. P. Winpenny and E. J. L. McInnes, *Angew. Chem. Int. Ed*. 2014, **53**, 5310.
8. X.-Y. Wang, C. Avendano and K. R. Dunbar, *Chem. Soc. Rev*., 2011, **40**, 3213.
9. L. Ungur and L. F. Chibotaru, Computational Modelling of the Magnetic Properties of Lanthanide Compounds, in: Lanthanides and Actinides in Molecular Magnetism, Ch. 6 (Wiley), in press.
10. K. S. Pedersen, J. Dreiser, J. Nehrkorn, M. Gysler, M. Schau-Magnussen, A. Schnegg, K. Holldack, R. Bittl, S. Piligkos, H. Weihe, P. Tregenna-Piggott, O. Waldmann and J. Bendix, *Chem. Commun*., 2011, **47**, 6918.
11. (a) S. K. Langley, N. F. Chilton, L. Ungur, B. Moubaraki, L. F. Chibotaru and K. S. Murray, *Inorg. Chem*., 2012, **51**, 11873; (b) S. K. Langley, N. F. Chilton, L. Ungur, B. Moubaraki, L. F. Chibotaru and K. S. Murray, *Inorg. Chem*., 2014, **53**, 4303.
12. S. K. Langley, D. P. Wielechowski, V. Vieru, N. F. Chilton, B. Moubaraki, B. F. Abrahams, L. F. Chibotaru and K. S. Murray, *Angew. Chem. Int. Ed*., 2013, **52**, 12014.
13. (a) J. D. Rinehart, M. Fang, W. J. Evans and J. R. Long, *Nature Chem*., 2011, **3**, 538; (b) S. Demir, J. M. Zadrozny, M. Nippe and J. R. Long, *J. Am. Chem. Soc*., 2012, **134**, 18546.
14. F. Aquilante, L. De Vico, N. Ferre, G. Ghigo, P.-A.Malmqvist, P. Neogrady, T. B. Pedersen, M. Pitonak, M. Reiher, B. O. Roos, L. Serrano-Andres, M. Urban, V. Veryazov and R. J. Lindh, *Comput. Chem*., 2010, **31**, 224.
15. F. Neese, U. Becker, F. Wennmohs, D. Ganiouchine and T. Petrenko, ORCA 2.9.0; http://cec.mpg.de/forum/
16. (a) B. O. Roos, P. R. Taylor and P. E. M. Siegbahn, *Chem. Phys*., 1980, **48**, 157; (b) See the MOLCAS manual: http://molcas.org/documentation/manual/node95.html; (c) L. F. Chibotaru and L. Ungur, *Chem. Phys*., 2012, **137**, 064112.
17. K. Yamaguchi Y. Takahara T. Fueno, V.H. Smith Ed. Applied Quantum Chemistry, V. Reidel, Dordrecht, 1986, 155.
18. M. E. J. Lines, *Chem. Phys*. 1971, 55, 2977.
19. L. Ungur, M. Thewissen, J.-P.Costes, W. Wernsdorfer and L. F. Chibotaru, *Inorg. Chem*., 2013, **52**, 6328.

